

## Aqueous Proton Transfer Across Single Layer Graphene

Jennifer L. Achtyl<sup>1</sup>, Raymond R. Unocic<sup>2</sup>, Lijun Xu<sup>4</sup>, Yu Cai<sup>4</sup>, Muralikrishna Raju<sup>5</sup>, Weiwei Zhang<sup>5</sup>, Robert L. Sacchi<sup>3</sup>, Ivan V. Vlassiuk<sup>3</sup>, Pasquale F. Fulvio<sup>3,6</sup>, Panchapakesan Ganesh<sup>7</sup>, David J. Wesolowski<sup>7</sup>, Sheng Dai<sup>7</sup>, Adri C. T. van Duin<sup>5</sup>, Matthew Neurock<sup>4</sup>, and Franz M.

Geiger<sup>1\*</sup>

<sup>1</sup>Department of Chemistry, Northwestern University, 2145 Sheridan Road, Evanston, IL 60201, USA.

<sup>2</sup>Center for Nanophase Materials Sciences Oak Ridge National Laboratory, Oak Ridge, TN 37831, USA.

<sup>3</sup>Measurement Science & System Engineering Division, Oak Ridge National Laboratory, Oak Ridge, TN 37931, USA.

<sup>4</sup>Departments of Chemical Engineering and Chemistry 102 Engineers' Way, University of Virginia, Charlottesville, VA 22904-4741, USA.

<sup>5</sup>Department of Mechanical and Nuclear Engineering, Pennsylvania State University, University Park, PA 16801, USA.

<sup>6</sup>Department of Chemistry, University of Puerto Rico, Río Piedras Campus; San Juan, 00931 PR.

<sup>7</sup>Chemical Sciences Division, Oak Ridge National Laboratory, Oak Ridge, Tennessee 37831, USA.

\*Correspondence and requests for materials should be addressed to F.M.G. (email: geigerf@chem.northwestern.edu).

### Abstract

Proton transfer across single layer graphene is associated with large computed energy barriers and is therefore thought to be unfavorable at room temperature unless nanoscale holes or dopants

are introduced, or a potential bias is applied. Here, we subject single layer graphene supported on fused silica to cycles of high and low pH and show that protons transfer reversibly from the aqueous phase through the graphene to the other side where they undergo acid-base chemistry with the silica hydroxyl groups. After ruling out diffusion through macroscopic pinholes, the protons are found to transfer through rare, naturally occurring atomic defects. Computer simulations reveal low energy barriers of 0.61 to 0.75 eV for aqueous proton transfer across hydroxyl-terminated atomic defects that participate in a Grotthuss-type relay, while pyrylium-like ether terminations shut down proton exchange. Unfavorable energy barriers to helium and hydrogen transfer indicate the transfer process is selective for aqueous protons.

## **Introduction**

Brick-and-mortar networks of stacked graphene oxide nanosheets can act as effective membranes<sup>1-8</sup> while single layer graphene exhibits dramatically lower permeabilities towards gases<sup>4,9</sup>. In fact, graphene is thought to be unfit even for proton transfer, which is associated with computed gas phase energy barriers exceeding 1.4 eV<sup>10</sup> unless dopants or nanoscale openings are externally introduced<sup>6,7,10,11</sup>, or an external potential bias is applied<sup>12</sup>. To determine whether graphene is indeed impermeable to protons, we placed well-characterized single layer graphene<sup>13</sup> on top of a fused silica substrate and cycled, at room temperature and constant ionic strength, the bulk pH of an aqueous solution above the graphene layer between basic and acidic (Supplementary Information). We tested for proton exchange through graphene by probing the underlying silica surface with an interfacial potential-dependent version of second harmonic generation (SHG, Figure 1a)<sup>14,15</sup> using 120 fsec input pulses at energies well below the graphene damage threshold<sup>13</sup>. With a detection limit of  $10^{-5}$  to  $10^{-6}$  V<sup>16</sup>, the method is sensitive enough to follow protonation or deprotonation of as little as 1% of the available silanol groups present in

the area probed by SHG. The interfacial potential vanishes at the point of zero charge (PZC of fused silica  $\sim 2.5$ )<sup>17</sup> and the SHG signal intensity is small<sup>14,18,19</sup>. Increasing the pH at constant ionic strength shifts the relevant interfacial acid-base equilibria  $\text{SiOH}_2^+ + \text{OH}^- \rightleftharpoons \text{SiOH} + \text{H}_2\text{O}$  and  $\text{SiOH} + \text{OH}^- \rightleftharpoons \text{SiO}^- + \text{H}_2\text{O}$  ( $\text{pK}_a \sim 4.5$  and  $\sim 8.5$ )<sup>14,18,20</sup> to the right and the resulting interfacial potential polarizes the interfacial water molecules such that the SHG signal intensity increases<sup>14,18</sup>. Intuitively, the close proximity of the graphene layer and the charged fused silica surface, combined with the sensitivity of the method, make our approach akin to an Å-scale voltmeter for detecting even rare occurrences of proton exchange. We find no significant difference between the SHG vs. time traces recorded in the presence and absence of graphene. After ruling out diffusion through macroscopic pinholes, the protons are found to transfer through rare, naturally occurring atomic defect sites. Computer simulations reveal low energy processes for water-mediated proton transfer across hydroxyl-terminated atomic defect sites that participate in a Grotthuss-type relay, while defects terminated by pyrylium-like ether bridges shut down proton exchange.

## Results

### Silanol protonation and deprotonation unimpeded by graphene.

Using a dual-pump flow system (Fig. 1a) at a flow rate of at  $\sim 0.9$  mL/sec, we varied the bulk solution pH between 3 to 10 while maintaining constant 1 mM ionic strength. As shown in Fig. 1b, we find no significant difference between the SHG vs. time traces recorded in the presence and absence of graphene, and no statistically significant differences in the kinetic rates and jump durations (Supplementary Tables S1 and S2). The SHG responses to pH changes are consistent with the acid-base equilibria of the fused silica/water interface<sup>14,15,19,21</sup>, yielding effective  $\text{pK}_{a,\text{eff}}$  values of 3.5(1) and 8.3(2), which fall within the reported literature values (Supplementary

Information section SIID)<sup>22</sup>. This finding indicates that the SHG experiments do not track merely ion adsorption to the graphene/water interface but acid-base chemistry at the fused silica surface underneath it, for which proton transfer across the membrane is a necessary condition. As expected from refs 1-5, porous graphene multilayers do not inhibit proton transfer either (Supplementary Information section SIIC). Based on these results we conclude that the fused silica/water interface does not behave differently in terms of relative surface charge density, in the duration of the jumps, or in the rates of the jumps when single layer graphene is present. These findings indicate that the acid/base chemistry at the fused silica/water interface occurs in an unimpeded fashion in the presence of single layer graphene.

#### **Importance of macroscopic defects ruled out.**

Scanning electron microscopy (SEM) images of graphene single layers deposited on fused silica windows show a low density of macroscopic pinholes and that the graphene is free of cracks or folds (Fig. 1c). Two-dimensional diffusion from those locations to the location of the laser beam is considered by calculating, for a given proton diffusion coefficient  $D$ , the mean-square displacement,  $\langle \Delta r^2 \rangle$ , according to  $\langle \Delta r^2 \rangle = z \cdot t \cdot D$ , where  $t$  is time and  $z$  is the number of neighboring sites to which the proton can hop<sup>23</sup> (six in for the case of the hexagonal graphene lattice). In the literature, reported theoretically and experimentally determined proton surface diffusion coefficients range between  $1.01 \times 10^{-7} \text{ cm}^2\text{s}^{-1}$  and  $9.00 \times 10^{-5} \text{ cm}^2\text{s}^{-1}$ <sup>24,39</sup>. While the bulk diffusion coefficient for a proton in water is accepted to range between  $8 \times 10^{-5} \text{ cm}^2/\text{s}$  and  $9 \times 10^{-5} \text{ cm}^2\text{s}^{-1}$ , there are disagreements in the literature about whether the surface proton diffusion coefficient is similar to the bulk coefficient or slower than the bulk coefficient on hydrophobic and hydrophilic surfaces for a variety of different systems<sup>24,28,39</sup>. Reactivity is expected to substantially slow down the 2D diffusion of the proton ( $\sim$  magnitude 20x reduction)<sup>30,40,41</sup> when it

moves across an amphoteric oxide whose protonation effectively terminates the diffusion path. Reactive proton diffusion coefficients reported for Nafion<sup>42,43</sup> are similarly low. Indeed, our own reactive force field calculations containing partially hydroxylated quartz surfaces show the proton diffusion is quickly terminated by protonation of the surface SiO<sup>-</sup> groups (Supplementary Fig. S2 and associated text). This result indicates that proton diffusion is significantly slower in the presence of surface anionic species due to proton trapping at these sites.

In our experiments, the continuous proton supply from the aqueous bulk is expected to form a propagating reaction front: our calculations show a drastically increased proton diffusion coefficient of  $4.944 \times 10^{-5} \text{ cm}^2\text{s}^{-1}$ , or just half of that of bulk water, once protons arriving through any opening within the graphene sheet interact with the hydroxylated portion of the surface that is located behind the reaction front. To conservatively assess an upper bound limit for our estimations, we calculated the proton mean square displacement using a D value of  $1 \times 10^{-6} \text{ cm}^2 \text{ s}^{-1}$ . The probability of placing our laser beam within the propagating reaction front emanating from a given macroscopic pinhole was then estimated to be 4 and 21% for 1 second and 10 second SHG jump times, respectively (Supplementary Information Table S3). Given that the pH jumps were repeated on least 18 different days with 8 different graphene samples and delays in changes of the SHG response were not observed with statistical significance, we conclude that the diffusion of protons from the few macroscopic pinholes that are present in our samples, or, alternatively, from the sample edge, to the area probed by the laser can not explain our observations of proton transfer through graphene.

### **The needle in the haystack: atomic defects.**

Scanning transmission electron microscopy (STEM) was then used to search for atomic defects using annular dark field (ADF) STEM imaging at 60 kV. The majority of the images show

perfect six-fold symmetry in the position of the carbon atoms and vast areas that lack grain boundaries and atomic, or vacancy, defects (Fig. 1d). Nevertheless, similar to prior reports of atomic scale vacancy point defects<sup>44,45</sup>, we find, albeit rarely, atomic defects (Fig. 1e). Unless hydrocarbons or heavy metal atoms<sup>46</sup> are present in graphene, defect formation due to electron beam-induced etching (as opposed to ion bombardment or oxidative etching)<sup>47</sup> of pristine CVD graphene at the energies employed here is unlikely. Rather, the rare defects we observe on occasion are more likely to originate from the synthesis process or cosmic rays, as the STEM experiments are carried out below the knock-on damage threshold for graphene<sup>48</sup>, and the femtosecond laser pulses are attenuated below the onset of processes other than SHG<sup>13</sup>. Given a lower limit to the estimated defect-to-defect distance of  $\sim 0.1 \mu\text{m}$ <sup>49</sup> (while difficult to determine accurately from Raman spectroscopy, the actual distance is likely to be longer), we assess the probability of placing our laser beam within the propagating reaction front emanating from a given atomic defect to be 100%.

## **Discussion.**

To elucidate the mechanisms for proton transfer, we discuss findings from density functional theory (DFT) calculations (Fig. 2) and ReaxFF reactive force field molecular dynamics (Fig. 3)<sup>50-</sup><sup>52</sup> simulations. DFT simulations track the detailed changes in the electronic structure and quantify corresponding activation barriers as protons transfer from the water layer through the graphene interface and exit into solution on the opposite side of the surface, whereas the ReaxFF simulations provide a more detailed representation of the interfaces and more rigorous accounting of the dynamics. We find that the main restriction for aqueous proton transfer through pristine, defect-free graphene is the energy required to push the proton into the center of the graphene. The water molecules above and below the graphene layer are unavailable for

participation in this process as the non-defective graphene surface is hydrophobic. The energy difference that is reported is due to the initial reference (or reactant) state. Release of the proton from an aquated hydronium ion towards the graphene layer is associated with an energy penalty of  $\sim 0.65$  eV as the initial O-H bond needs to be broken, as shown in frame two of Supplementary Fig. S12.

In the presence of atomic scale defect sites the barrier to aqueous proton transfer through graphene was calculated to decrease from over 3.0 eV to under 1.0 eV (Table I). The simulations indicate that the proton transfers from the solution phase to the surface through the center of the defect site and into the solution on the opposite side of the membrane via a Grotthuss<sup>53</sup> mechanism involving proton shuttling. The solution phase proton shuttling paths occur with barriers of  $< 0.2$  eV, whereas the barrier to transfer through a given defect site is somewhat higher due to limited access of water and OH groups required for proton shuttling.

The quad vacancy site is found to be the smallest defect site that facilitates proton transfer through graphene (Table I). This site is comprised of 6 coordinatively unsaturated carbon atoms that are either terminated with 3 oxygen atoms in epoxide-like arrangements reminiscent of pyrylium cations (different from the crown ethers recently reported by Guo et al.)<sup>54</sup>, or with 6 hydroxide groups. Supporting Fig. S23 shows all considered defect terminations are energetically favorable as compared to the bare quad-vacancy system. Proton transfer through the pyrylium-terminated 4V site requires 1.7 eV (Fig. 2a), attributed to the protophobicity of pyrylium cations and their in-plane localization, which leaves a 3.4 Å gap between water and the graphene substrate that prevents proton transfer. The hydroxyl-terminated site, however, provides hydrogen bonding conduits via a Grotthuss mechanism that lowers the barrier to proton transfer to somewhere between 0.61 eV (ReaxFF) and 0.68 eV (DFT, Fig. 2b), indicating it will

occur at room temperature. Additional ReaxFF simulations shows that a water channel, which establishes itself upon proton transfer, thins and finally vanishes when the pairs of OH groups terminating the defect site are successively replaced with oxygen atoms (Fig. 3a-d). These transfer paths are selective to aqueous protons as helium and H<sub>2</sub> transfer requires barriers exceeding 1.9 eV (Supplementary Fig. S19).

We conclude that aqueous protons transfer through single layer graphene via rare, OH-terminated atomic defects at room temperature. While the rarity of the atomic defect sites would make it challenging to follow proton exchange across graphene using pH-sensitive electrodes, the close proximity of the graphene layer and the charged fused silica surface, where the experimental observation of surface protonation and deprotonation is made by SHG, allows for the experimental observation of proton exchange across these rare defects. The associated energy barriers are comparable to experimentally determined activation energy barriers for proton transfer through graphene subjected to an externally applied potential<sup>12</sup>. From the SHG signal jump rates and the times required for 2D proton diffusion, we estimate that the presence of as few as a handful of atomic defects in a 1  $\mu\text{m}^2$  area sample of single layer graphene is sufficient to allow for the apparent unimpeded protonation and deprotonation of the interfacial silanol groups within ten seconds. Yet, we caution that given the limited accuracy with which the defect density can be determined in large (mm)-scale graphene, aqueous protons may transfer across single layer graphene not only along the path discussed here, but others as well. The identification of low barriers specifically for water-assisted transfer of protons through OH-terminated atomic defects in graphene, and high barriers for oxygen-terminated defects could be an important step toward the preparation of zero-crossover proton-selective membranes.



## Methods.

We used graphene having a grain size of  $\sim 100 \mu\text{m}^{55}$  grown on copper foils by atmospheric pressure CVD<sup>55,56</sup>. The graphene was transferred using spincoating of poly(methyl methacrylate) (PMMA) followed by copper etching in a  $\text{FeCl}_3$  solution and PMMA removal in acetone. The transfer was made onto clean fused silica substrates (ISP Optics, 1" diameter, QI-W-25-1, flatness 1 wave per inch at 633 nm) to fill approximately one  $\text{cm}^2$  with a single layer. Following annealing in a flow of 4%  $\text{H}_2$  in Ar for 30 min at 300 °C, vibrational sum frequency generation spectra showed no evidence for CH stretches<sup>57</sup>. Similar to the fining of water layers between graphene and mica by atomic force microscopy<sup>58</sup>, there is probably water located between the graphene samples and the fused silica substrates used here.

In the SHG experiments, we accessed the aqueous/graphene/fused silica interface through the fused silica substrate at a kHz repetition rate with 120 fsec pulses having a wavelength of 600 nm and with energies of 0.15  $\mu\text{J}$  and 0.3  $\mu\text{J}$  for graphene and silica, respectively (see Supporting Information section SIII). Correct power dependencies and spectral responses are verified regularly, the SHG responses are well polarized, and sample damage does not occur<sup>57,59</sup>. UV-vis and Raman spectra shown in the Supplementary Information indicate that the samples are resistant to acid-base cycling under the conditions employed here. The aqueous solutions were prepared with Millipore water, prepared the day prior to an experiment and left open to air overnight to equilibrate with atmospheric  $\text{CO}_2$ , and NaCl (Alfa Aesar, 99+%). The concentration of NaCl was confirmed using a conductivity meter (Fisher Traceable Conductivity and TDS meter, Fisher Scientific). Solution pH was adjusted with minimum amounts of dilute solutions of  $\sim 1\text{M}$  NaOH (Sigma-Aldrich, 99.99%) and HCl (EMD ACS grade).

ReaxFF, DFT, and ab initio molecular dynamics calculations were carried out as described in detail in the Supporting Information section SV. Given the importance of surface relaxation in atomically defected graphene layers<sup>60</sup>, all of our calculations on the 1, 2, and 4V carbon vacancy sites and the oxygen-terminated sites explicitly modeled surface relaxation.

**Online Content.** Any additional methods, extended data display items, and source data are available in the online version of the paper; references unique to these sections appear only in the online paper.

**Acknowledgments:** This work was supported by the Fluid Interface Reactions, Structures and Transport (FIRST) Center, an Energy Frontier Research Center funded by the U.S. Department of Energy, Office of Science, Office of Basic Energy Science.

**Author Contributions.** F.M.G. conceived of the idea. J. L. A., R. R. U., R.L.S., I.V.V., and P. F. F. performed the experiments. L.X., Y.C., M.R., W.Z., G.P., A. C. T. v. D. and M.N. performed the computational work. The manuscript was written with substantial contributions from all authors.

#### **Additional Information**

**Competing financial interests.** The authors declare no competing financial interests.

## References and Notes:

- 1 Joshi, R. K. *et al.* Precise and Ultrafast Molecular Sieving Through Graphene Oxide Membranes. *Science* **343**, 752-754, (2014).
- 2 Mi, B. Graphene Oxide Membranes for Ionic and Molecular Sieving. *Science* **343**, 740-742, (2014).
- 3 Gao, W. *et al.* Ozonated Graphene Oxide Film as a Proton-Exchange Membrane. *Angew. Chemie Int. Ed.* **53**, 1-6, (2014).
- 4 Nair, R. R., Wu, H. A., Jayaram, P. N., Grigorieva, I. V. & Geim, A. K. Unimpeded Permeation of Water Through Helium-Leak-Tight Graphene-Based Membranes. *Science* **335**, 442-444, (2012).
- 5 Guo, F. *et al.* Graphene-based environmental barriers. *ES&T* **46**, 7717-7724, (2012).
- 6 Hauser, A. W. & Schwerdtfeger, P. Nanoporous Graphene Membranes for Efficient <sup>3</sup>He/<sup>4</sup>He Separation. *J. Phys. Chem. Lett.* **3**, 209-213, (2011).
- 7 Banerjee, S. *et al.* Electrochemistry at the Edge of a Single Graphene Layer in a Nanopore. *ACS Nano* **7**, 834-843, (2013).
- 8 Wang, X. D. *et al.* Atomistic Origins of High Rate Capability and Capacity of N - Doped Graphene for Lithium Storage. *Nano Lett.* **14**, 1164-1171, (2014).
- 9 Bunch, J. S. *et al.* Impereable Atomic Membranes from Graphene Sheets. *Nano Lett.* **8**, 2458-2462, (2008).
- 10 Miao, M., Nardelli, M. B., Wang, Q. & Liu, Y. First principles study of the permeability of graphene to hydrogen atoms. *PCCP* **15**, 16132-16137, (2013).
- 11 Jiang, D., Cooper, V. R. & Dai, S. Porous graphene as the ultimate membrane for gas separation. *Nano Lett.* **9**, 4019-4024, (2009).
- 12 Hu, S. *et al.* Proton transport through one-atom-thick crystals. *Nature* **516**, 227-230, (2014).
- 13 Achtyl, J. L. *et al.* Free Energy Relationships in the Electrical Double Layer over Single-Layer Graphene. *J. Am. Chem. Soc.* **135**, 979-981, (2013).
- 14 Ong, S., Zhao, X. & Eissenthal, K. B. Polarization of water molecules at a charged interface; second harmonic studies of the silica/water interface. *Chem. Phys. Lett.* **191**, 327-335, (1992).
- 15 Gibbs-Davis, J. M., Kruk, J. J., Konek, C. T., Scheidt, K. A. & Geiger, F. M. Jammed Acid-Base Chemistry at Interfaces. *J. Am. Chem. Soc.* **130**, 15444-15447, (2008).
- 16 Konek, C. T. *et al.* Interfacial Acidities, Charge Densities, Potentials, and Energies of Carboxylic Acid-Functionalized Silica/Water Interfaces Determined by Second Harmonic Generation. *J. Am. Chem. Soc.* **126**, 11754-11755, (2004).
- 17 Stumm, W. & Morgan, J. J. *Aquatic Chemistry, Chemical Equilibria and Rates in Natural Waters*. 3rd edn, (John Wiley & Sons, 1996).
- 18 Higgins, S. R., Stack, A.G., Knauss, K.G., Eggleston, C.M., Jordan, G. Probing molecular-scale adsorption and dissolution-growth processes using nonlinear optical and scanning probe methods suitable for hydrothermal applications. *Geochemical Society Special Publication No. 7*, 111, (2002).

- 19 Azam, M. S., Weeraman, C. N. & Gibbs-Davis, J. M. Halide-Induced Cooperative Acid–Base Behavior at a Negatively Charged Interface. *J. Phys. Chem. C* **117**, 8840-8850, (2013).
- 20 Duval, Y., Mielczarski, J. A., Pokrovsky, O. S., Mielczarski, E. & Ehrhardt, J. J. Evidence of the Existence of Three Types of Species at the Quartz-Aqueous Solution Interface at pH 0-10: XPS Surface Group Quantification and Surface Complexation Modeling. *J. Phys. Chem. B.* **106**, 2937-2945, (2002).
- 21 Stack, A. G., Higgins, S. R. & Eggleston, C. M. Point of zero charge of a corundum-water interface probed with optical second harmonic generation (SHG) and atomic force microscopy (AFM): New approaches to oxide surface charge. *Geochim. Cosmochim. Acta* **65**, 3055-3063, (2001).
- 22 Azam, M. S., Weeraman, C. N. & Gibbs-Davis, J. M. Specific Cation Effects on the Bimodal Acid–Base Behavior of the Silica/Water Interface. *The Journal of Physical Chemistry Letters* **3**, 1269-1274, (2012).
- 23 Oura, K. L., V.G.; Saranin, A.A.; Zotov, A.V.; Katayama, M.;. *Surface Science: An Introduction.* (Springer, 2003).
- 24 Zhang, C. *et al.* Water at hydrophobic interfaces delays proton surface-to-bulk transfer and provides a pathway for lateral proton diffusion. *Proceedings of the National Academy of Sciences*, (2012).
- 25 Alexiev, U. M., R.; Scherrerr, P.; Khorana, H.G.; Heyn, M.P.;. Rapid long-rang proton diffusion along the surface of the purple membrane and delayed proton transfer into the bulk. . *PNAS* **92**, 372-376, (1995).
- 26 Antoneko, Y. N. P., P.;. Microinjection in combination with microfluorimetry to study proton diffusion along phospholipid membranes. *Eur Biophys J* **37**, 865-870, (2008).
- 27 Brändén, M., Sandén, T., Brzezinski, P. & Widengren, J. Localized proton microcircuits at the biological membrane–water interface. *Proceedings of the National Academy of Sciences* **103**, 19766-19770, (2006).
- 28 Slevin, C. J. & Unwin, P. R. Lateral Proton Diffusion Rates along Stearic Acid Monolayers. *J. Am. Chem. Soc.* **122**, 2597-2602, (2000).
- 29 Soroka, H. P. *et al.* Excited-State Proton Transfer and Proton Diffusion near Hydrophilic Surfaces. *J. Phys. Chem. C* **117**, 25786-25797, (2013).
- 30 Choi, P., Jalani, N. H. & Datta, R. Thermodynamics and Proton Transport in Nafion: II. Proton Diffusion Mechanisms and Conductivity. *J. Electrochem. Soc.* **152**, E123-E130, (2005).
- 31 Atkins, P. d. P., J.;. *Atkins' Physical Chemistry.* Eighth Edition edn, (W.H. Freeman and Company, 2006).
- 32 Heberle, J. R., J.; Thiedemann, G.; Oesterheld, D.; Dencher, N.A.;. Proton migration along the membrane surface and retarded surface to bulk transfer. *Nature* **370**, 370-382, (1994).
- 33 Springer, A., Hagen, V., Cherepanov, D. A., Antonenko, Y. N. & Pohl, P. Protons migrate along interfacial water without significant contributions from jumps between ionizable groups on the membrane surface. *Proceedings of the National Academy of Sciences*, (2011).

- 34 Iuchi, S., Chen, H., Paesani, F. & Voth, G. A. Hydrated Excess Proton at Water–Hydrophobic Interfaces†. *The Journal of Physical Chemistry B* **113**, 4017-4030, (2008).
- 35 Smondyrev, A. M. & Voth, G. A. Molecular Dynamics Simulation of Proton Transport Near the Surface of a Phospholipid Membrane. *Biophys. J.* **82**, 1460-1468, (2002).
- 36 Kudin, K. N. & Car, R. Why Are Water–Hydrophobic Interfaces Charged? *J. Am. Chem. Soc.* **130**, 3915-3919, (2008).
- 37 Zhang, J. U., P.R.;. Scanning electrochemical microscopy (SECM) feedback approach for measuring lateral proton diffusion in langmuir monolayers: theory and application. *Phys. Chem. Chem. Phys.* **4**, 3814-3819, (2002).
- 38 Tuckerman, M. E., Chandra, A. & Marx, D. Structure and Dynamics of OH-(aq). *Acc. Chem. Res.* **39**, 151-158, (2006).
- 39 Yamashita, T. & Voth, G. A. Properties of Hydrated Excess Protons near Phospholipid Bilayers. *The Journal of Physical Chemistry B* **114**, 592-603, (2009).
- 40 Junge, W. M., S.;. The role of fixed and mobile buffers in the kinetics of proton movement. *Biochim. Biophys. Acta* **890**, 1-5, (1987).
- 41 Eikerling, M., Kornyshev, A. A., Kuznetsov, A. M., Ulstrup, J. & Walbran, S. Mechanisms of Proton Conductance in Polymer Electrolyte Membranes. *The Journal of Physical Chemistry B* **105**, 3646-3662, (2001).
- 42 Choi, P., Jalani, N. H. & Datta, R. Thermodynamics and Proton Transport in Nafion II. Proton Diffusion Mechanisms and Conductivity. *J. Electrochem. Soc.* **152**, E123-E130, (2005).
- 43 Petersen, M. K. & Voth, G. A. Characterization of the Solvation and Transport of the Hydrated Proton in the Perfluorosulfonic Acid Membrane Nafion. *J. Phys. Chem. B*, 18594-18600, (2006).
- 44 Hashimoto, A., Suenaga, K., Gloter, A., Urita, K. & Iljima, S. Direct evidence for atomic defects in graphene layers. *Nature* **430**, 870-873, (2004).
- 45 Meyer, J. C. *et al.* Direct Imaging of Lattice Atoms and Topological Defects in Graphene Membranes. *Nano Lett.* **8**, 3582-3586, (2008).
- 46 Zan, R., Ramasse, Q. M., Bangert, U. & Novoselov, K. S. Graphene Reknits Its Holes. *Nano Lett.* **12**, 3936-3940, (2012).
- 47 O'Hern, S. C. *et al.* Selective Ionic Transport through Tunable Subnanometer Pores in Single-Layer Graphene Membranes. *Nano Lett.* **14**, 1234-1241, (2014).
- 48 Meyer, J. C. *et al.* Accurate Measurement of Electron Beam Induced Displacement Cross Sections for Single-Layer Graphene. *Phys. Rev. Lett.* **108**, 196102, (2012).
- 49 Achtyl, J. A., Vlassiuk, I. V., Dai, S. & Geiger, F. M. Interactions of Organic Solvents at Graphene/  $\alpha$ -Al<sub>2</sub>O<sub>3</sub> and Graphene Oxide/  $\alpha$ -Al<sub>2</sub>O<sub>3</sub> Interfaces Studied by Sum Frequency Generation. *J. Phys. Chem. C* **118**, 17745-17755, (2014).
- 50 Kresse, G. & Furthmuller, J. Efficient iterative schemes for ab initio total energy calculations using a plane-wave basis set. *Phys. Rev. B* **54**, 11169-11186, (1996).
- 51 van Duin, A. C., Dasgupta, S., Lorant, F. & Goddard, W. A. ReaxFF: A Reactive Force Field for Hydrocarbons. *J. Phys. Chem. A* **105**, 9396-9409, (2001).

- 52 Baustian, K. J. *et al.* Importance of aerosol composition, mixing state, and morphology for heterogeneous ice nucleation: A combined field and laboratory approach. *Journal Of Geophysical Research-Atmospheres* **117**, (2012).
- 53 de Grotthuss, C. J. T. Sur la décomposition de l'eau et des corps qu'elle tient en dissolution à l'aide de l'électricité galvanique. *Ann. Chim.* **58**, 54-73, (1806).
- 54 Guo, J. *et al.* Crown ethers in graphene. *N. Comm.* **5**, 5389, (2014).
- 55 Vlassiouk, I. *et al.* Graphene Nucleation Density on Copper: Fundamental Role of Background Pressure. *J. Phys. Chem. C* **117**, 18919-18926, (2013).
- 56 Huang, P. *et al.* Grains and grain boundaries in single-layer graphene atomic patchwork quilts. *Nature* **469**, 389-392, (2010).
- 57 Achtyl, J. L. *et al.* Interaction of Magnesium Ions with Pristine Single-Layer and Defected Graphene/Water Interfaces Studied by Second Harmonic Generation. *J. Phys. Chem. B*, (2014).
- 58 Xu, K., Cao, P. & Heath, J. R. Graphene Visualizes the First Water Adlayers on Mica at Ambient Conditions. *Science* **329**, 1188-1191, (2010).
- 59 Achtyl, J. L. *et al.* Free energy relationships in the electrical double layer over single-layer graphene. *J. Am. Chem. Soc.* **135**, 979-981, (2013).
- 60 Buettner, M., Choudhury, P., Johnson, J. K. & Yates, J. T. Vacancy clusters as entry ports for cesium intercalation in graphite. *Carbon* **49**, 3937-3952, (2011).

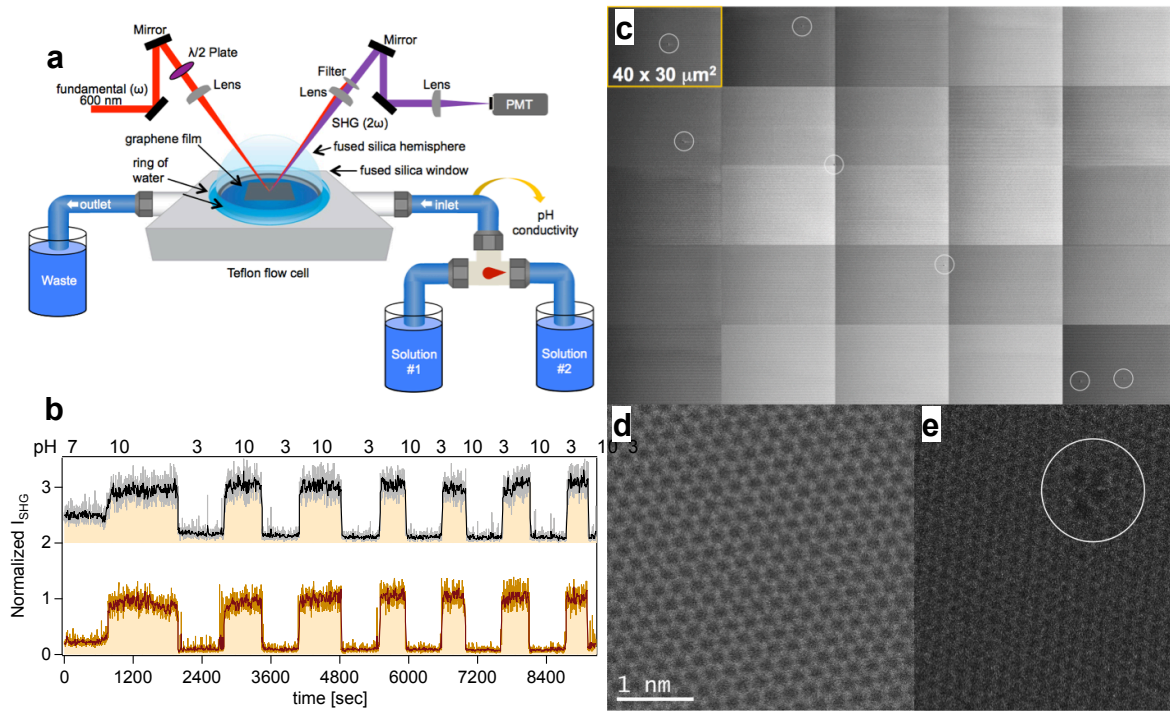


**Fig. 1. Experimental approach.** (a) Experimental setup using a waveplate ( $\lambda/2$ ) to prepare 600 nm light plane-polarized parallel to the plane of incidence (p-in) while a photomultiplier tube (PMT) detects the second harmonic generation (SHG) photons at  $\lambda=300$  nm. (b) p-in/all-out Polarized SHG response recorded as a function of time from the fused silica/water interface during pH jumps from 7 to 3 to 10 and subsequent pH cycling between 3 and 10 at a bulk aqueous flow of 0.9 mL/sec and 1 mM NaCl concentration in the absence (crimson, bottom) and presence (black, top, offset for clarity) of single layer graphene placed between the fused silica substrate and the flowing bulk aqueous phase. 5-Point boxcar indicated by dark lines. (c) Composite of 25 SEM images of single layer graphene on a fused silica substrate, showing 7 macroscopic pinholes, marked by white circles. (d) High resolution aberration-corrected ADF STEM

images of defect-free single layer graphene on a TEM grid and (e) of a rarely imaged atomic defect.



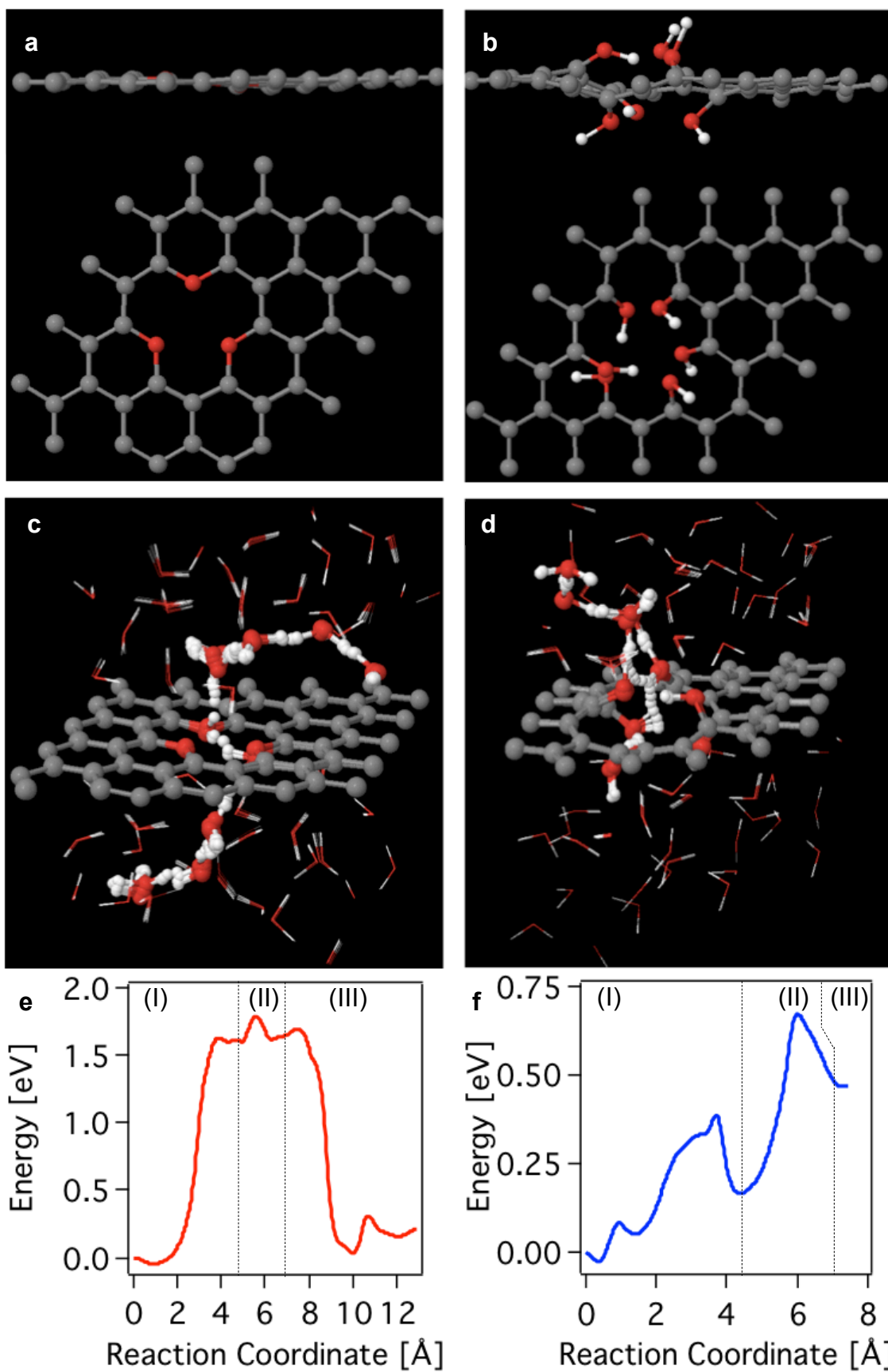


**Fig. 2. Density Functional Theory Calculations.** Side and top views of oxygen- (a) and OH-(b) terminated defect models used in the DFT calculations. Snapshots (c, d) and energetics (e, f) from the nudged elastic band calculations for proton transfer through the ether- and OH- terminated defect sites marking (**region I**) release of proton from  $\text{H}_3\text{O}^+$  to ether and OH group, respectively; (**region II**) relay of proton between ether and OH groups, respectively; (**region III**) release of proton from ether and OH groups to  $\text{H}_3\text{O}^+$ , respectively. Denotations of spheres: grey=carbon; red=oxygen; white=hydrogen atoms.

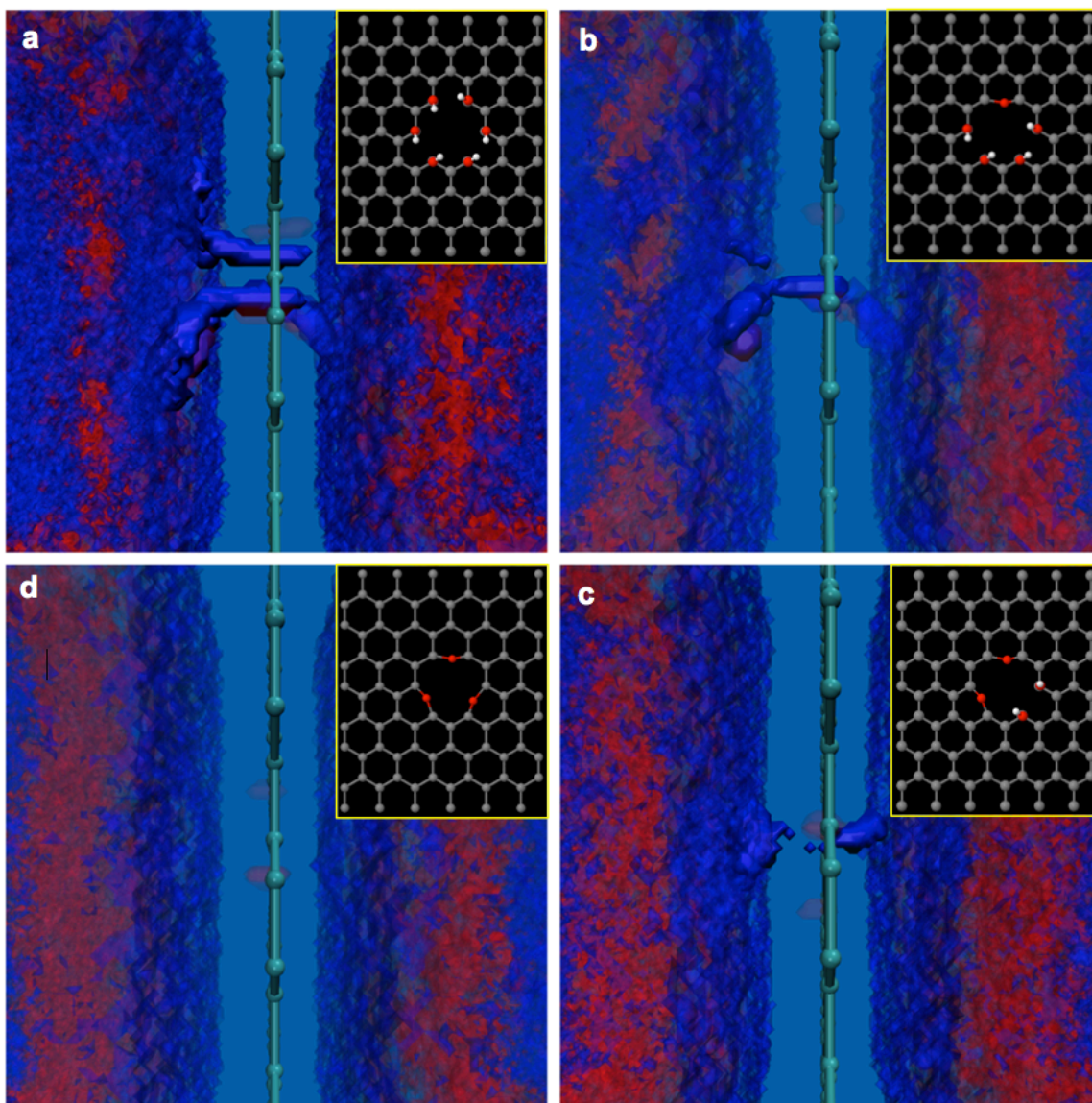


**Fig. 3. Reactive Force Field calculations.** Water channel formation from ReaxFF calculations of water mediated proton transfer through atomic defects terminated in 6 OH groups (a), 4 OH groups and one oxygen atom (b), 2 OH groups and two oxygen atom (c), and three oxygen atoms (d). Denotations of spheres: grey=carbon; red=oxygen; white=hydrogen atoms.

**Table I****DFT and ReaxFF-calculated activation barriers for proton transfer through different vacancy sites on graphene in water**

Graphene Surface	Bottom Layer	Defect Termination	Activation Barrier <i>DFT</i>	Activation Barrier <i>ReaxFF</i>
No vacancy	water	No termination	3.9 eV	Not computed
1V	water	No termination	> 2.0 eV	3.54 eV
4V	water	No termination	0.25 eV	0.22 eV
4V	water	3O ether capped	1.8 eV	1.7 eV
4V	water	6OH hydroxyl capped	0.68 eV	0.61 eV
4V	Water + SiO <sub>2</sub>	3O ether capped	2.5 eV	2.53 eV
4V	Water + SiO <sub>2</sub>	6OH hydroxyl capped	0.7 eV	0.75 eV